



Evaluating the responses of alluvial and bedrock aquifers to earthquakes (M_L 5.1 and M_L 5.8) using hydrological and environmental tracer data

Dugin Kaown¹ · Dong-Chan Koh^{2,3} · Heejung Kim¹ · Hee Jae Koh² · Jaeyeon Kim¹ · Sanghoon Lee¹ · Inwoo Park¹ · Kang-Kun Lee¹

Received: 30 August 2018 / Accepted: 13 March 2019 / Published online: 5 April 2019
© Springer-Verlag GmbH Germany, part of Springer Nature 2019

Abstract

In Gyeongju, South Korea, local magnitude M_L 5.1 and M_L 5.8 earthquakes occurred on 12 September 2016; M_L 4.5 aftershocks and >500 aftershocks with $M_L > 1.5$ were observed over the next 3 months. Responses of the aquifers were compared using hydrological and environmental tracer data (noble gases, $\delta^{18}\text{O}$, δD , ^3H , and ^{13}C). To assess the hydrologic response to the earthquake activity by the shallow (alluvial) and deep (bedrock) aquifers, time series data from the national groundwater monitoring wells were compared. Groundwater-level changes were not observed in most alluvial wells, while groundwater level and electrical conductivity (EC) increased in the confined igneous rock for several days to months after the earthquake activity. Noble gas anomalies in groundwater were closely related to the epicentral distance, lithology, and aquifer type. The relatively low concentration of ^3H (<0.8 TU) and depleted values of $\delta^{18}\text{O}$ and δD in the alluvial and bedrock aquifers suggest they were affected by upwelling of deep and old water. Elevated values of $\delta^{13}\text{C}$ and ^{222}Rn were observed in wells close to the epicenter. Groups resulting from cluster analysis using environmental tracer data were closely related to the responses of the earthquake on the aquifers of different types (alluvial and bedrock), lithologies, and distances from the epicenter. Groundwater-level change and geochemical response after the earthquake activity showed different correlations depending on aquifer and fault types. Combined use of groundwater level, EC, and environmental tracer data in groundwater can be useful to understand the origin and preferential flow paths of water during and after earthquakes.

Keywords Earthquake · Environmental tracer · Noble gas · Radon · South Korea

Introduction

On September 12, 2016, two earthquakes of local magnitude M_L 5.1 and M_L 5.8 occurred at 10:44:32 and 11:32:55 UTC approximately 1 h apart in Gyeongju, South Korea. The M_L 5.8

event was the largest magnitude earthquake since the start of earthquake monitoring with modern instrumental recording networks in South Korea. The earthquake occurred along the Yangsan Fault System in the Gyeongsang Basin. The Yangsan Fault System includes the NNE–SSW-trending Yangsan Fault and a series of branching faults. Detailed information on the earthquakes can be found in Kim et al. (2016). It is difficult to understand seismic activity near the Yangsan Fault System based on short-term earthquake data, but considering long-term historical earthquake data for about 2,000 years, several researchers have mentioned relatively high seismic activity near the Yangsan Fault System (Lee and Jin 1991).

There have been many studies related to changes in groundwater level before and after earthquakes (Gau et al. 2007; Manga and Wang 2007; Amoruso et al. 2011; Niwa et al. 2012; Lee et al. 2013; Shi and Wang 2015; Lee 2016; Liu et al. 2018; Petitta et al. 2018). The redistribution of stress

✉ Kang-Kun Lee
kklee@snu.ac.kr

¹ School of Earth and Environmental Sciences, Seoul National University, Seoul 08826, Republic of Korea

² Korea Institute of Geoscience and Mineral Resources, Daejeon 34132, Republic of Korea

³ University of Science and Technology, Daejeon 34113, Republic of Korea

and strain induced by an earthquake can change the groundwater level during the earthquake (Montgomery and Manga 2003; Liu et al. 2018). The groundwater level response to an earthquake is affected by the magnitude, depth of the hypocenter, and distance from the well to the epicenter. Thus, groundwater levels can oscillate during the passage of the seismic waves, or they can show sustained changes from a few days to several months depending on the aquifer characteristics (Montgomery and Manga 2003; Wang and Manga 2010; Niwa et al. 2012; Pavin et al. 2014; Yan et al. 2014; Liu et al. 2018).

Changes in the geochemistry of groundwater before and after an earthquake can be caused by the result of seismically induced changes in the hydraulic properties of the crust (Claesson et al. 2004; Ingebritsen and Manga 2014; Skelton et al. 2014). Changes to groundwater flow paths and geochemistry prior to or after an earthquake can be explained by the fluid pressure changes caused by earthquake stress, which can cause changes in the permeability fields (Manga 2001; Song et al. 2005; Reddy and Nagabhushanam 2012). The inflow of new groundwater induced by an earthquake can affect geochemical properties by changing the fluid sources and stimulating water–rock interactions caused by alteration between fracture pathways due to permeability structure changes induced by seismic waves (Claesson et al. 2004; Elkhoury et al. 2006; Skelton et al. 2014; Andr n et al. 2016; Barberio et al. 2017; Galassi et al. 2014). Radon count rates, the values of $\delta^{18}\text{O}$ and δD isotopes, and the concentrations of Na^+ , Ca^{2+} , Si , Cl^- , SO_4^{2-} , and transition metals, show variations after earthquakes (Igarashi et al. 1995; Skelton et al. 2014; Andr n et al. 2016).

Radiogenic noble gases such as ^4He and ^{40}Ar are accumulated in mineral grains due to the decay of radioactive elements and move into the pore fluid by diffusion (Torgersen and Clarke 1985; Lehmann et al. 2003; Bauer et al. 2016). Released radiogenic noble gases have been used as a new tracer to analyze stress and strain in aquifers (Umeda and Ninomiya 2009; Bauer et al. 2016). Therefore, noble gases in groundwater have been usefully applied to evaluate mixing processes and the origins of water in many studies (Tolstikhin et al. 1996; Sano et al. 2015, 2016; Tomonaga et al. 2017). The atmospheric $^3\text{He}/^4\text{He}$ ratio is 1.384×10^{-6} and ^3He and ^4He can be produced in the crust. The nonatmospheric noble gases can be tritogenic ^3He (produced by the decay of ^3H), terrigenous ^4He , and ^3He from the solid earth (Schlosser et al. 1988; Solomon and Cook 2000). Terrigenous $^3\text{He}/^4\text{He}$ and anomalies after earthquakes have been studied by many researchers (Umeda and Ninomiya 2009; Newell et al. 2015; Sano et al. 2015, 2016; Tomonaga et al. 2017). The $^3\text{He}/^4\text{He}$ ratio has been applied to identify sources of terrigenous ^4He (Kipfer et al. 2002; Tomonaga et al. 2017); additionally, ^4He has also been applied to assess mixing of old and young water in faults, as ^4He is a very sensitive tracer to identify upward

movement of old water through faults (Batlle-Aguilar et al. 2017).

The Gyeongju earthquake was small compared to large earthquakes in the world, but it was the largest earthquake ever experienced by Koreans living in the country, and thus became a national concern. The reason for the Koreans' special concern is that existing nuclear power plants and a newly planned nuclear power plant site are located about 50 km away from the Gyeongju earthquake epicenter. Although the Yangsan Fault System was recognized as having a high probability of causing an earthquake in Korea, there has been no major earthquake for decades, so there was no hydrogeological monitoring around the Yangsan Fault System before the Gyeongju earthquake. Fortunately, some observation wells in the national groundwater monitoring network are located near the Gyeongju earthquake epicenter and time series of water levels, electrical conductivity (EC), and geochemical data have been collected.

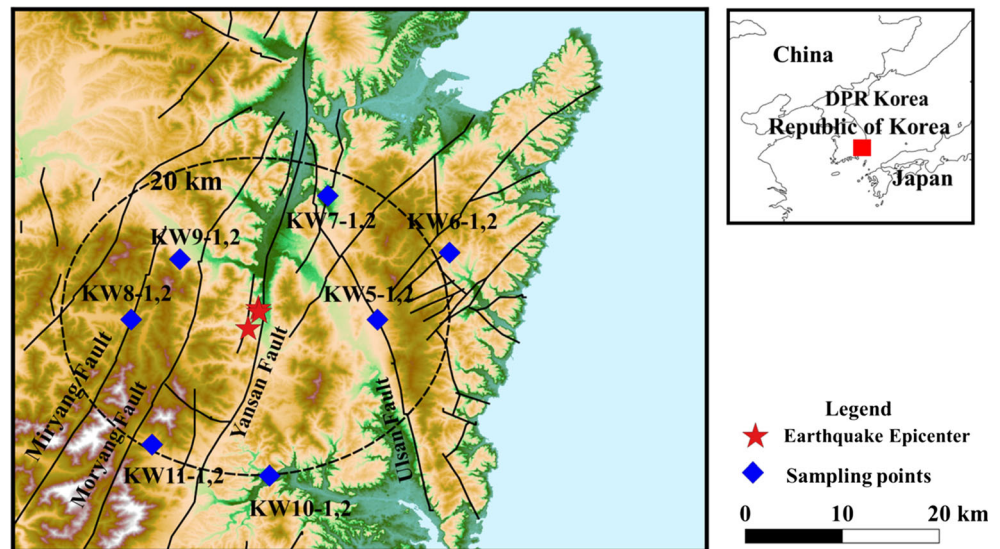
The purpose of this study is to understand how and when groundwater can reflect earthquake influences. Based on the water level data and the distance between the epicenter and the monitoring wells, target wells and reference wells were selected for this study. Using the selected wells, hydrogeochemical and isotopic analyses were carried out to investigate relationships between parameters, the earthquake, and geological properties. A new approach presented in this study is the combined assessment of hydrologic and geochemical responses to an earthquake, considering different types of faults and lithologies. Combined use of groundwater level, EC, and geochemical change and environmental tracer data (^3H , $^3\text{He}/^4\text{He}$, $\delta^{13}\text{C}$, $\delta^{18}\text{O}$, and δD) were evaluated to understand hydrologic and geochemical responses to earthquakes in alluvial and bedrock aquifers composed of sedimentary, igneous, and metamorphic rock.

Materials and methods

Study area

Two consecutive earthquakes ($M_L 5.1$ and $M_L 5.8$) occurred along a buried strike-slip fault at a depth of 11–16 km in Gyeongju on September 12, 2016, and more than 500 aftershocks up to $M_L 4.5$ occurred (Hong et al. 2017). Gyeongju is located 300 km away from Seoul, Korea (Fig. 1). The southeastern part of the Korean Peninsula mainly consists of the Cretaceous Gyeongsang Supergroup, Upper Cretaceous to Paleogene granites, and Neogene sediments (Chough and Sohn 2010). The Gyeongsang Supergroup is divided into three major lithological units, the lower Sindong, the middle Hayang and the upper Yucheon groups (Chang 1975). The study area, where the $M_L 5.8$ Gyeongju Earthquake occurred, consists of the Yucheon Group, the Paleogene Namsan alkali

Fig. 1 Monitoring wells in the study area



granite, and the Neogene Yeonil Group. The Yucheon Group mainly comprises andesitic to rhyolitic volcanic rocks and clastic to volcanic clastic sediments juxtaposed tectonically along the Yangsan Fault (Kim et al. 1971). The Neogene Yeonil Group, bounded by the Yangsan Fault, is comprised of siliciclastic sediments. The Yangsan Fault acts as a boundary fault for both the Yucheon Group and the opening of the Miocene Pohang Basin. The southeastern part of Korea shows a distinctive NNE-directed geomorphological feature with several strike-slip fault systems including the Ilkwang, Dongrae, Yangsan, Morayng, and Milyang faults. The M_L 5.8 Gyeongju Earthquake occurred along the N30 °E-directed hidden branch fault of the Yangsan Fault Zone (Hong et al. 2017). Wells KW8 and KW11 are located close to the Yangsan Fault. Wells KW7 and KW5 are located close to the Ulsan Fault, which is a reverse fault and where the epicenters of the aftershocks were mainly located (Kim et al. 2016).

Seven national groundwater monitoring stations are located around the epicenter and a pair of wells with different depths are installed at each station. Seven shallow wells (6.8–26 m) are installed in the alluvial aquifer, and seven deep wells (60–100 m) are located in the bedrock aquifer at each monitoring station. The alluvial aquifers are composed of sedimentary rock such as sand, gravel, and pebbles, while the bedrock aquifers are composed of shale, mudstone, and conglomerate, except for at locations KW8-2 and KW11-2, where the composition is igneous rock (Table 1). The aquifers in the eastern part of the study area located in the Ulsan fault (reverse fault) area are composed of sedimentary rock such as sand, gravel, pebbles, mudstone, and conglomerate, while aquifers in the western part of the study area located in the Yangsan, Morayng, and Milyang fault (strike-slip fault) area are composed of igneous rock.

Methods

The depth to the water table ranges from 0.72 to 7.8 m; the depth to the water table, aquifer type, and lithology of the aquifers are shown in Table 1. Data loggers were installed in the national groundwater monitoring stations to measure groundwater level, EC, pH, and temperature hourly throughout the year. Hydrogeochemical data were measured at the national groundwater monitoring stations in 2014 (16 September to 29 October) and 2015 (25 August to 18 November) before the M_L 5.1 and M_L 5.8 Gyeongju earthquake. After the earthquake, hydrogeochemical data were analyzed at the same wells in 2016 (19 September–18 October) and 2017 (16–18 January). Groundwater samples for environmental tracers were collected from 14 wells in January 2017 including seven wells from the alluvial aquifer and seven wells from the bedrock aquifer (Fig. 1). A YSI probe (USA) was used to measure pH, electrical conductivity (EC), temperature, dissolved oxygen (DO), and salinity in the field. Water samples were collected using a Grundfos pump (Denmark) after three well volumes of water were pumped, allowing EC, temperature, and DO to stabilize. Water samples were filtered (0.45 μ m) and collected in 50-ml bottles for anion analysis and $\delta^{18}\text{O}$ and δD isotope analysis. Samples for cation analysis were acidified using HNO_3 . HCO_3^- was measured using the gran titration method in the field. Samples for tritium analysis were collected in 1-L plastic bottles, while samples for noble gas analysis were collected using copper tubes with metal pinch clamps. Groundwater samples for $\delta^{13}\text{C-DIC}$ (dissolved inorganic carbon) were collected in 50-ml bottles, and samples for ^{222}Rn were collected in triplicate in 130-ml bottles.

Cation and anion concentrations were measured using inductively coupled plasma atomic emission spectrometry (ICP) and ion chromatography at the Korea Basic Science Institute.

Table 1 Characteristics of wells around the epicenter

Well	Aquifer type	Elevation (m asl)	Total depth (m)	Depth to water table (m)	Depth of screened interval (m)	Geology
KW5-1	Alluvial	96.8	12.5	4.7	8.0–10.0	Quaternary sand/gravel
KW5-2	Bedrock	96.8	100	5.96	34–38, 50–54, 58–62, 74–78, 82–86	Paleogene alkali granite
KW6-1	Alluvial	136.22	26	4.15	22.0–26.0	Quaternary sand/gravel
KW6-2	Bedrock	136.22	73	4.37	54.0–58.0, 58.0–62.0, 62.0–66.	Neogene Yeonil mudstone
KW7-1	Alluvial	41.38	8.8	2.6	3.8–7.8	Quaternary pebbles
KW7-2	Bedrock	42.38	60	2.52	48.0–60.0	Neogene Yeonil conglomerate
KW8-1	Alluvial	200.04	6.8	1.25	1.8–5.8	Quaternary pebbles
KW8-2	Bedrock	200.04	65	0.72	41.0–53.0	Cretaceous Yucheon andesite
KW9-1	Alluvial	89.07	12	3.08	8.0–12.0	Quaternary sand/gravel
KW9-2	Bedrock	89.09	70	3.1	50.0–54.0, 58.0–62.0, 66.0–70.0	Cretaceous Hayang shale
KW10-1	Alluvial	23.76	19.2	7.66	7.5–11.5	Quaternary silt/sand
KW10-2	Bedrock	23.72	79	7.81	24.0–28.0, 32.0–36.0, 40.0–44.0	Cretaceous Hayang shale
KW11-1	Alluvial	198.56	13.5	5.14	8.5–12.5	Quaternary silt/sand
KW11-2	Bedrock	198.59	60	3.73	24.0–28.0, 32.0–36.0, 40.0–44.0	Cretaceous granite

The values of $\delta^{18}\text{O}$ and δD were measured using a VG prism II stable isotope ratio mass spectrometer at the Korea Basic Science Institute, and reported using δ notation relative to the Vienna Standard Mean Ocean Water (V-SMOW) with precisions of $\pm 0.1\text{‰}$ for $\delta^{18}\text{O}$ and $\pm 1\text{‰}$ for δD (Lee and Lee 1999). The concentrations of ^{222}Rn were measured using radon/thoron monitor RTM1688-2 (SARAD, Germany) in the field within 1 day of sampling.

The concentrations of ^3He , ^4He , ^{20}Ne , ^{40}Ar , ^{83}Kr , and ^{131}Xe were measured using a magnetic sector field mass spectrometer (215-50) at the University of Utah with 1% precision for $^3\text{He}/^4\text{He}$ and ^4He , 2% precision for ^{20}Ne and ^{40}Ar , and 4% precision for ^{83}Kr and ^{131}Xe . Tritium concentrations were measured using the liquid scintillation counting method at the University of Waterloo, Canada, with a detection limit of 0.6 TU (tritium units). The values of $\delta^{13}\text{C}$ were measured using a MicroGas-IsoPrime mass spectrometer at the University of Waterloo and reported relative to IAEA carbonate standards with the precisions of 0.2‰. An annual average air temperature of 13.4 °C was assumed for the infiltrated water temperature in the saturated zone and used for the $^{20}\text{Ne}/^4\text{He}$ ratio in air-saturated water.

Cluster analysis can identify groups of similar variables using a multivariate dataset. In hydrogeochemical studies, cluster analysis groups variables with similar physical and geochemical properties in a groundwater system (Kaown et al. 2007; Kim et al. 2018). Wells KW10-1 and KW10-2 were not included in the cluster analysis since noble gas data were not analyzed in those wells. The measured data were standardized for the cluster analysis to equalize the influence of each parameter; cluster analysis was conducted using R software version 3.4.3.

Results

Groundwater levels and electrical conductivity

In the study area, most wells in the alluvial aquifer and some wells in the bedrock aquifer showed a rapid response to precipitation, while wells KW8-2 and KW11-2 did not show a rapid response to precipitation indicating characteristics of a confined aquifer. Groundwater level and EC changes after the earthquake in each well are shown in Table 2. After the earthquake, in most wells in the study area such as at KW5-1 and KW5-2, groundwater levels and EC oscillated slightly and then recovered within a few days (Fig. 2); however, in the bedrock aquifer at location KW8-2, groundwater levels increased, and the increase was sustained for several months after the earthquake (Fig. 2). In KW11-2, groundwater level decreased before the earthquake

Table 2 Water level and EC change in each well after the earthquake

Aquifer	Sample ID	Aquifer type ^a	Groundwater-level change	EC
Alluvial	KW5-1	u	Sustained	Negative
	KW7-1	u	Sustained	Negative
	KW8-1	u	Sustained	Negative
	KW11-1	u	Sustained	Negative
Bedrock	KW5-2	c	Sustained	Sustained
	KW7-2	u	Positive	Negative
	KW8-2	c	Positive	Sustained
	KW11-2	c	Positive	Positive

^a u unconfined, c confined

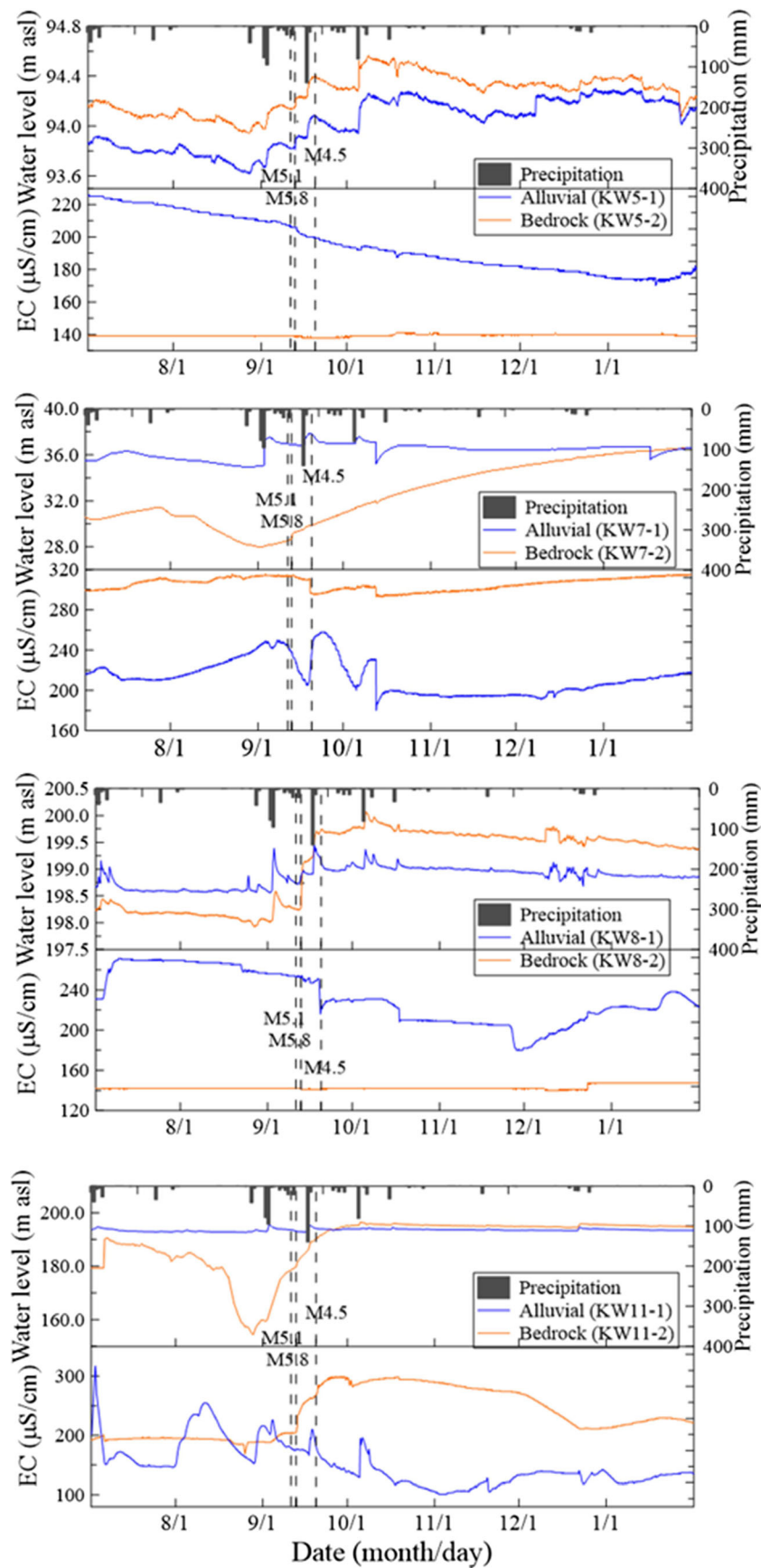


Fig. 2 Groundwater monitoring results from July 2016 to January 2017 in the selected wells: KW5-1, KW5-2, KW7-1, KW7-2, KW8-1, KW8-2, KW11-1, and KW11-2. Dashed lines indicate earthquakes

and increased after the earthquake (Fig. 2). The groundwater levels in the confined bedrock aquifers (KW8-2 and KW11-2) increased by 1.5 and 15 m, respectively after the earthquake. This result is consistent with previous study results, showing that increased groundwater levels were sustained from a few days to several months in confined aquifers after earthquakes (Montgomery and Manga 2003; Niwa et al. 2012; Shi and Wang 2015; Liu et al. 2018). The groundwater level in KW7-2 did not respond immediately but slowly increased for 3 months after the earthquake without any response to precipitation during that time, which is possibly related to the high frequency of the earthquake aftershocks along the Ulsan Fault near KW7-2 (Kim et al. 2016).

In most of the wells, EC did not respond to the earthquake except at KW7-2 and KW11-2. EC in KW7-2 decreased from 310 to 290 $\mu\text{S cm}^{-1}$ right after the earthquake of M_L 4.5 and gradually returned to the original EC (Fig. 2). The EC in KW11-2 increased from 205 to 300 $\mu\text{S cm}^{-1}$ after the earthquake. The increased groundwater level and EC in KW11-2 after the earthquake is likely related to the fact that this well was affected by upwelling of deep water. The increased EC and groundwater level in the bedrock aquifer after the earthquake is closely related to the earthquake derived stress (King et al. 2000; Orihara et al. 2014).

Stable isotope and tritium

The values of $\delta^{18}\text{O}$ and δD in groundwater samples from the alluvial and bedrock aquifers are compared in Fig. 3. In the bedrock aquifer, the values of $\delta^{18}\text{O}$ and δD in groundwater were depleted compared to those in the alluvial aquifer. Usually, the values of $\delta^{18}\text{O}$ and δD in groundwater are depleted in old groundwater recharged at high elevation (Crossey et al. 2009; Reddy et al. 2011; Skelton et al. 2014; Andr en et al. 2016). All samples deviated from the local meteoric water line. The values of $\delta^{18}\text{O}$ and δD were clustered into two groups: alluvial groundwater and bedrock groundwater. In the alluvial aquifer, the values of $\delta^{18}\text{O}$ and δD of groundwater and stream water were enriched, while the values of $\delta^{18}\text{O}$ and δD of groundwater from the bedrock aquifer were depleted. The values of $\delta^{18}\text{O}$ and δD in some wells responded after the earthquake, which is consistent with the results of Skelton et al. (2014).

The lowest values of $\delta^{18}\text{O}$ and δD were observed in KW8-2 which is located close to the fault and showed increased groundwater level after the earthquake (Fig. 2). Groundwater samples KW8-1 and KW11-1, which were collected from the alluvial aquifer, were clustered with the bedrock aquifer samples showing depleted values of $\delta^{18}\text{O}$ and δD , possibly indicating mixing with deep water. Groundwater sample KW7-1 did not fit into either group but was located between the two groups, indicating mixing between the groups. Samples from

Fig. 3 The values of $\delta^{18}\text{O}$ and δD in the alluvial and bedrock aquifers. The local meteoric water lines (LMWL) are shown

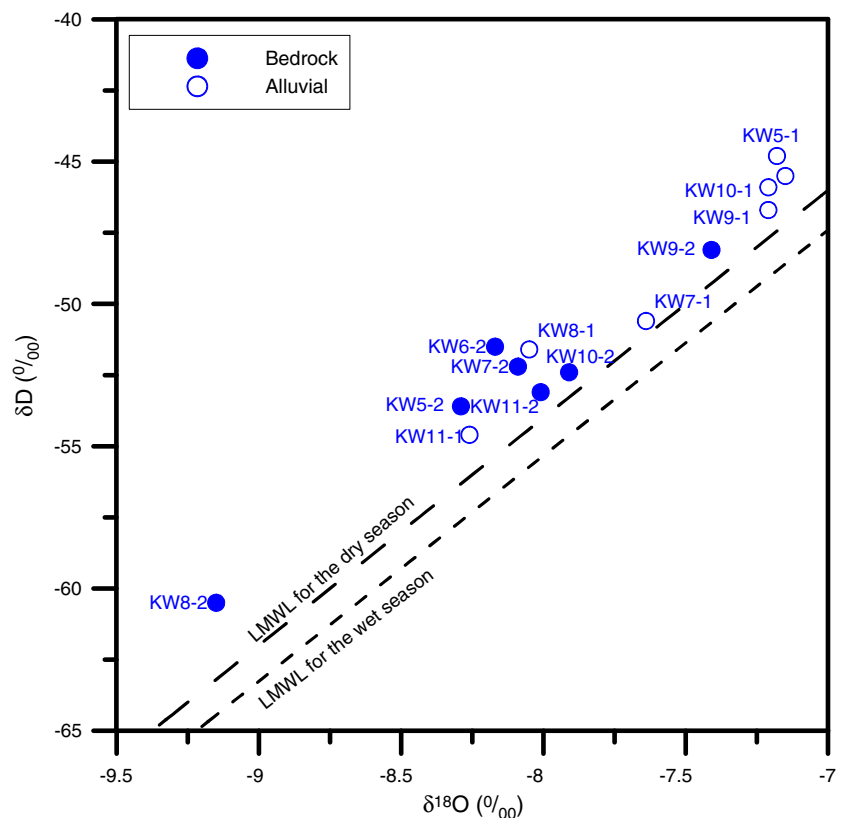


Table 3 Measured hydrogeochemical parameters and noble gas data in groundwater samples collected around the epicenter

Aquifer Sample ID	T °C	pH	DO	EC $\mu\text{S/cm}$	Ca	K	Mg	Na	Cl	SO ₄	NO ₃	HCO ₃	Rn Bq/L	$\delta^{18}\text{O}$ ‰	δD ‰	^3H TU	$\delta^{13}\text{C}$ ‰	Ar total (ccSTP/g)	Ne total (ccSTP/g)	Kr total (ccSTP/g)	Xe total (ccSTP/g)	^4He (ccSTP/g)	R/ R _a
Alluvial																							
KW5-1	15.4	7.52	2.24	213.1	17.7	2.67	7.07	13.0	9.45	49.5	13.5	31.2	15,849	-7.15	-45.5	3.7	-12.72	3.68E-04	1.97E-07	8.82E-08	1.20E-08	5.83E-08	1.09
KW6-1	15	6.87	0.64	315.5	1.76	3.79	0.99	74.4	21.6	26.0	0.28	124	225	-7.18	-44.8	10.2	-17.17	4.44E-04	2.37E-07	1.06E-07	1.49E-08	7.02E-08	0.69
KW7-1	16.1	7.29	0.8	180.1	15.8	0.91	5.75	15.7	11.1	2.47	1.15	90.2	1,218	-7.64	-50.6	0.8	-15.24	4.32E-04	2.26E-07	1.02E-07	1.38E-08	6.45E-08	0.98
KW8-1	11.5	7.01	1.63	224.7	19.1	6.36	3.91	19.2	22.2	16.8	15.9	57.7	5,974	-8.05	-51.6	3.3	-14.48	4.44E-04	2.19E-07	1.13E-07	1.62E-08	6.78E-08	0.84
KW9-1	14.3	7.02	5.17	513	53.6	16.9	21.6	12.3	18.4	46.6	40.9	187	585	-7.21	-46.7	4.4	-14.96	3.76E-04	2.00E-07	9.02E-08	1.23E-08	4.71E-08	0.99
KW10-1	17.2	7.69	7.05	294.7	29.2	4.23	6.50	21.0	22.5	31.3	19.2	76.6	228	-7.21	-45.9	NA	NA	NA	NA	NA	NA	NA	NA
KW11-1	14.9	7.21	6.98	121.5	11.7	2.11	1.93	8.38	7.04	13.1	12.8	32.6	4,204	-8.26	-54.6	3.3	-13.77	3.86E-04	1.97E-07	9.34E-08	1.30E-08	4.80E-08	1.02
Bedrock																							
KW5-2	15.6	6.55	0.74	309.7	30.5	2.43	5.11	35.2	17.7	27.9	0.3	137.1	17,575	-8.29	-53.6	0.8	-13.29	4.46E-04	2.29E-07	1.06E-07	1.48E-08	1.01E-06	1.31
KW6-2	14.9	8.15	0.69	530	1.6	1.75	0.68	145.6	33.8	17.0	0.14	257.0	368	-8.17	-51.5	0.8	-17.04	4.31E-04	2.36E-07	1.04E-07	1.45E-08	7.48E-08	0.70
KW7-2	15.1	7.01	2.76	140.3	9.9	0.98	3.7	15.8	9.6	2.7	1.9	68.2	992	-8.09	-52.2	0.8	-16.26	4.83E-04	4.44E-07	1.09E-07	1.45E-08	1.47E-07	1.02
KW8-2	14.6	7.3	0.82	146.8	12.6	0.33	2.01	18.4	3.5	15.3	0.8	64.3	23,060	-9.15	-60.5	0.8	-15.34	4.52E-04	2.53E-07	1.05E-07	1.50E-08	1.47E-07	0.59
KW9-2	14.9	6.9	0.58	521	62.3	10.4	24.0	13.3	18.5	43.7	38.9	204.1	249	-7.41	-48.1	4.8	-15.01	3.78E-04	2.06E-07	9.20E-08	1.26E-08	4.86E-08	1.00
KW10-2	16.3	7.07	2.2	865	94.8	2.2	13.2	92.6	15.4	305.2	10.2	160.5	758	-7.91	-52.4	NA	NA	NA	NA	NA	NA	NA	NA
KW11-2	15	7.07	0.96	227.3	32.5	1.4	2.1	13.0	7.6	34.6	4.1	79.5	488	-8.01	-53.1	3.3	-14.85	4.17E-04	2.54E-07	9.93E-08	1.32E-08	1.33E-07	0.44

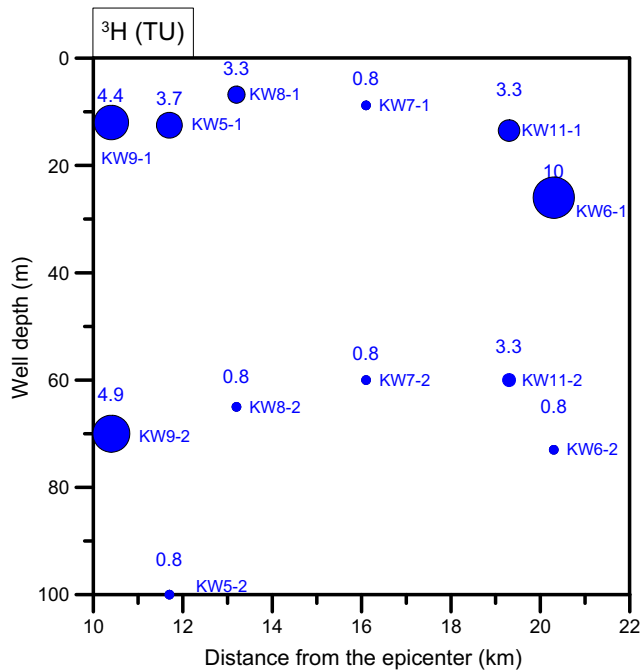


Fig. 4 Concentrations of tritium in the alluvial and bedrock aquifers

KW9-1 and KW9-2 showed similar values of $\delta^{18}\text{O}$ and δD , and KW9-2, located in the bedrock aquifer, was clustered with the alluvial aquifer samples. The similar values of $\delta^{18}\text{O}$ and δD in KW9-1 and KW9-2 might indicate mixing between these aquifers.

The concentration of tritium in the deeper wells is generally low (<0.8 TU), which can be an indicator of old water (Table 3). Tritium concentrations ranged from 0.8 to 10.2

TU in the alluvial aquifer and from 0.8 to 4.9 TU in the bedrock aquifer (Fig. 4), whereas the concentrations of ^3H in KW5-2, KW6-2, KW7-2, and KW8-2 were less than 0.8 TU. Groundwater samples collected in KW7-1 and KW7-2 all showed ^3H concentration below 0.8 TU, even though KW7-1 was collected at 10 m below the surface in a pebble aquifer (Fig. 4). Most recently recharged groundwater, collected from depths of 10–50 m, show ^3H concentrations of 2–10 TU in Korea (Kaown et al. 2009, 2014, 2018; Koh et al. 2012, 2018). The low concentration of ^3H in KW7-1 is likely due to upwelling of deep water in the shallow well, which is consistent with the change in EC in KW7-1 (Fig. 2).

Noble gas data

The $^3\text{He}/^4\text{He}$ ratio in the groundwater was compared with the distance to the epicenter for each well in the alluvial and bedrock aquifers (Fig. 5a). A decreasing $^3\text{He}/^4\text{He}$ ratio was observed with increasing distance from the epicenter, whereas similar values of $^3\text{He}/^4\text{He}$ were observed in the alluvial and bedrock aquifer in KW6 and KW9 (Fig. 5a). However, higher $^3\text{He}/^4\text{He}$ was observed in KW5-2 and KW7-2 in the bedrock aquifer compared to the alluvial aquifer in those locations, while lower $^3\text{He}/^4\text{He}$ was observed in KW8-2 and KW11-2 in the bedrock aquifer compared to the alluvial aquifer.

Ratios of $^{20}\text{Ne}/^4\text{He}$ and $^3\text{He}/^4\text{He}$ are compared in Fig. 5b. Low values of both $^{20}\text{Ne}/^4\text{He}$ and $^3\text{He}/^4\text{He}$ were observed after the earthquake in KW8-2 and KW11-2. This is likely caused by additional radiogenic helium sources in the crust mixed with an air component derived from the mixing of

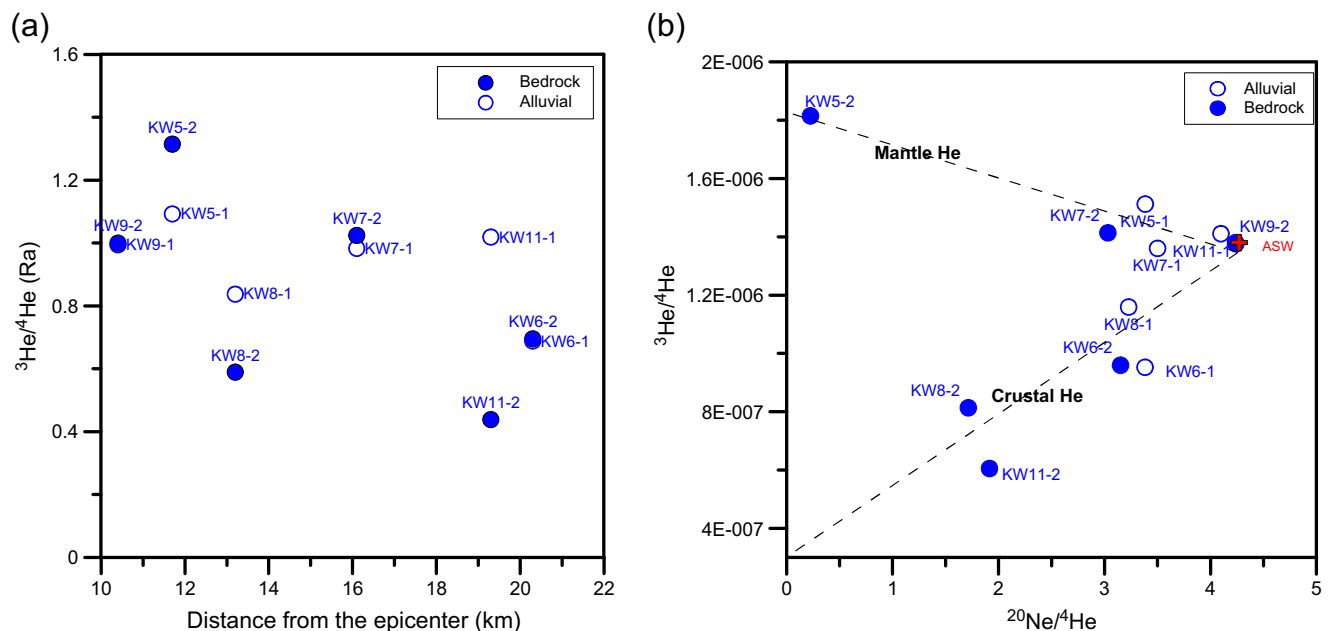


Fig. 5 $^3\text{He}/^4\text{He}$ ratio in groundwater in the alluvial and bedrock aquifers. a $^3\text{He}/^4\text{He}$ versus distance from the epicenter and b $^3\text{He}/^4\text{He}$ versus $^{20}\text{Ne}/^4\text{He}$

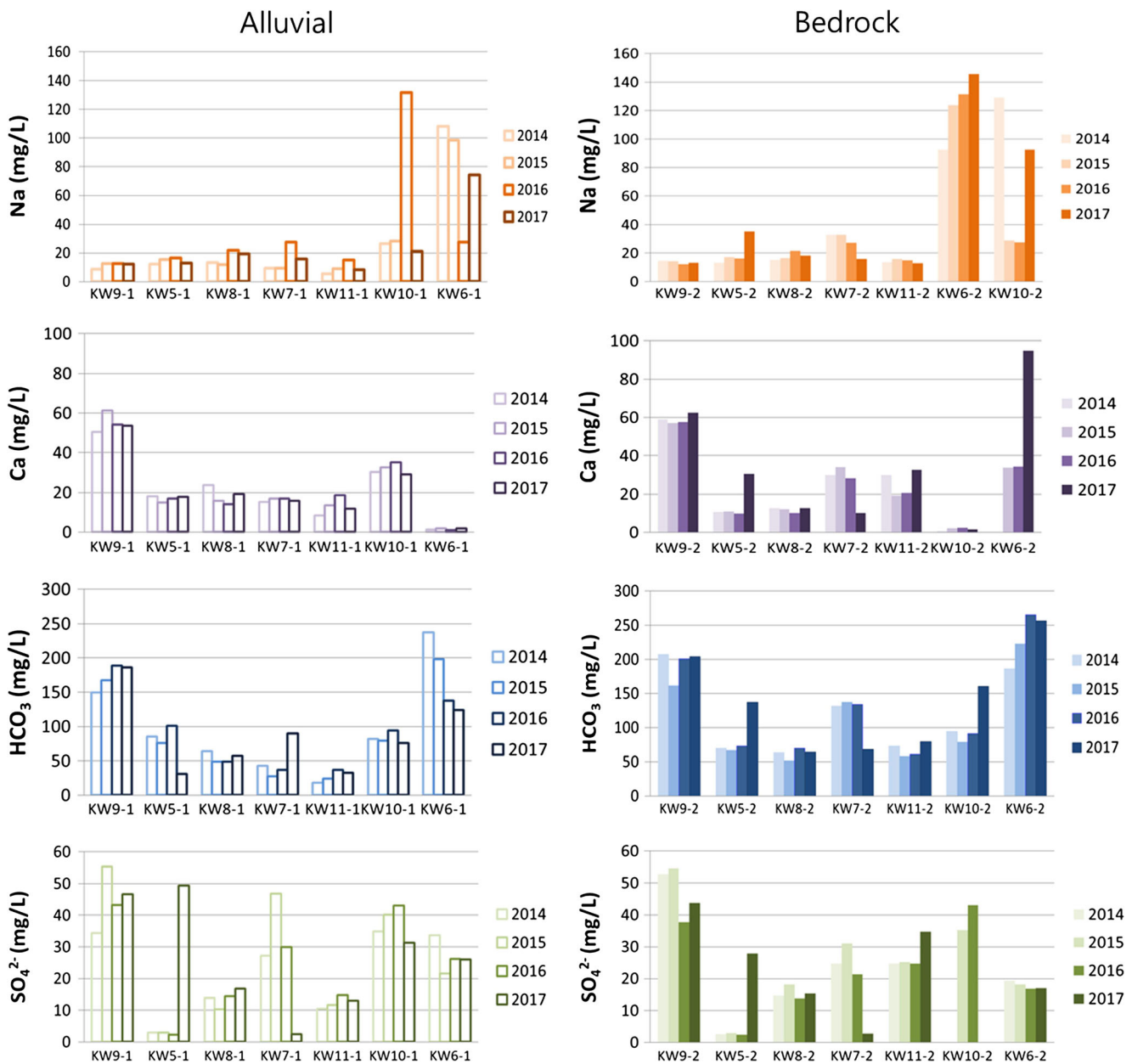


Fig. 6 Geochemical changes after the earthquake for groundwater from the alluvial and bedrock aquifers

shallow groundwater and air-saturated groundwater. However, the high $^3\text{He}/^4\text{He}$ ratio and low $^{20}\text{Ne}/^4\text{He}$ ratio observed in KW5-2 and KW7-2 can be explained by the addition of mantle ^3He due to fluid flow through the fracture (Fig. 5b).

Hydrogeochemical data

The concentrations of Na^+ , Ca^{2+} , SO_4^{2-} and HCO_3^- were compared in groundwater samples from the alluvial and bedrock aquifers before and after the earthquake (Fig. 6). In wells KW5, KW7, and KW10, the concentrations of Ca^{2+} , Na^+ , SO_4^{2-} , and HCO_3^- changed after the earthquake (Fig. 6).

Piper plots using concentrations of Ca^{2+} , Na^+ , K^+ , Mg^{2+} , Cl^- , SO_4^{2-} , and HCO_3^- show that groundwater from the bedrock aquifer was predominantly SO_4^{2-} and HCO_3^- type, and groundwater from the alluvial aquifer had a higher proportion of Cl^- (Fig. 7). The concentrations of Ca^{2+} , Na^+ , SO_4^{2-} , and HCO_3^- were higher in groundwater from the bedrock aquifer compared to the alluvial aquifer. Higher concentrations of NO_3^- and Cl^- were observed in groundwater from the alluvial aquifer compared to those of bedrock aquifer, since NO_3^- and Cl^- mainly originated from anthropogenic sources (Table 3). However, KW9-2, in the bedrock aquifer, showed high concentrations of NO_3^- , which is likely related to mixing between

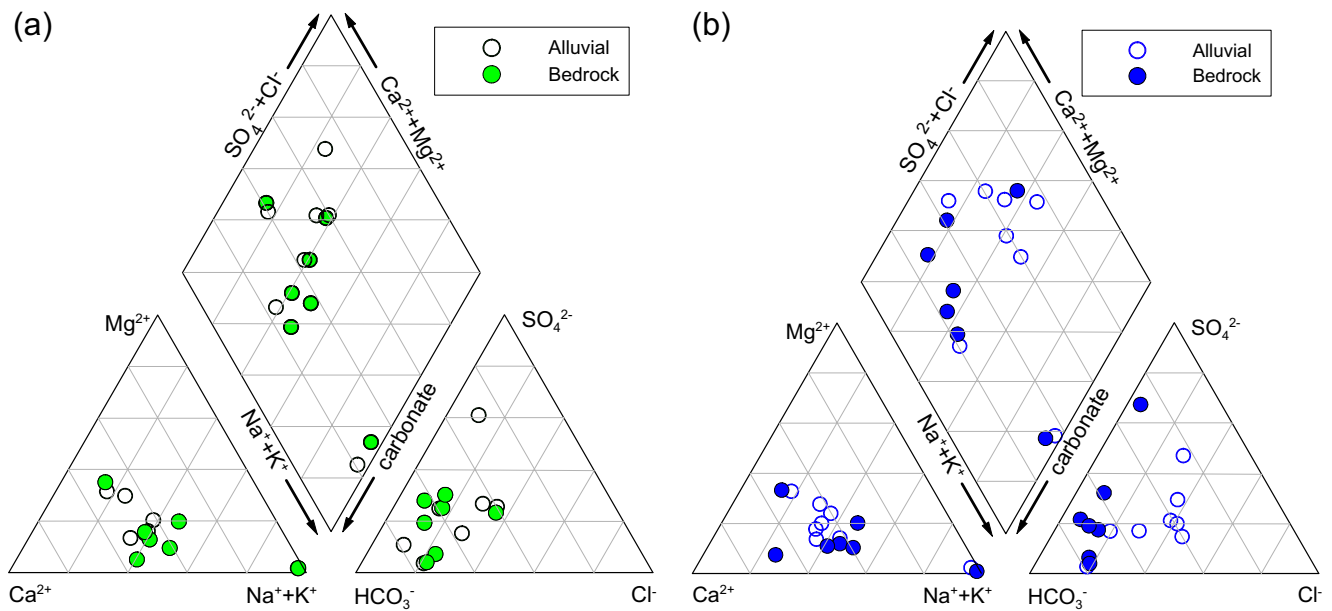


Fig. 7 Piper diagrams for groundwater from the alluvial and bedrock aquifers **a** before and **b** after the earthquake

the shallow and deep water. After the earthquake, the concentrations of Na^+ , Cl^- , and SO_4^{2-} increased in wells KW6-2 and KW10-2, which are located closer to the sea (Fig. 1).

High concentrations of ^{222}Rn were found in KW8-2 and KW5-2 in the bedrock aquifers, and ^{222}Rn concentrations decreased with increasing distance from the epicenter (Fig. 8a). KW6-2 and KW10-2, located close to the sea, showed low concentrations of ^{222}Rn . Decreasing values of $\delta^{13}\text{C}$ were also observed with increasing distance from the epicenter (Fig. 8a), whereas usually, values of $\delta^{13}\text{C}$ in soil range from -25 to

-22‰ and $\delta^{13}\text{C}$ from CO_2 in deep water range from -8 to -4‰ (Weise et al. 2001; Crossey et al. 2009; Saby et al. 2016). Depleted $\delta^{13}\text{C}$ -DIC is observed in recently recharged waters while enriched $\delta^{13}\text{C}$ -DIC is observed in deep and old waters determined by the ^3H - ^3He method (Saby et al. 2016). The concentrations of ^{222}Rn and values of $\delta^{13}\text{C}$ showed close correlations with epicentral distance in the study area.

The values of $\delta^{13}\text{C}$ were compared with ^{222}Rn concentrations to differentiate the input sources of CO_2 (Fig. 9a). Enriched $\delta^{13}\text{C}$ and higher concentrations of ^{222}Rn were

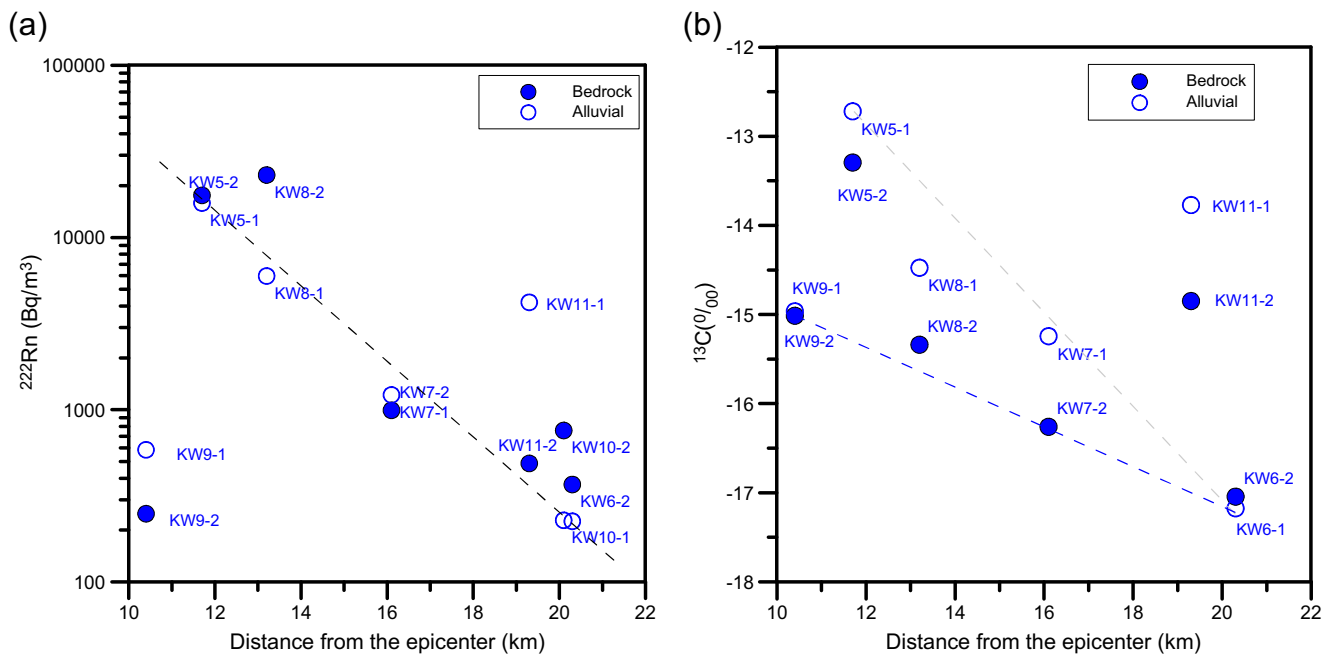


Fig. 8 The concentration values of **a** ^{222}Rn and **b** $\delta^{13}\text{C}$ in the groundwater samples, versus distance from the epicenter

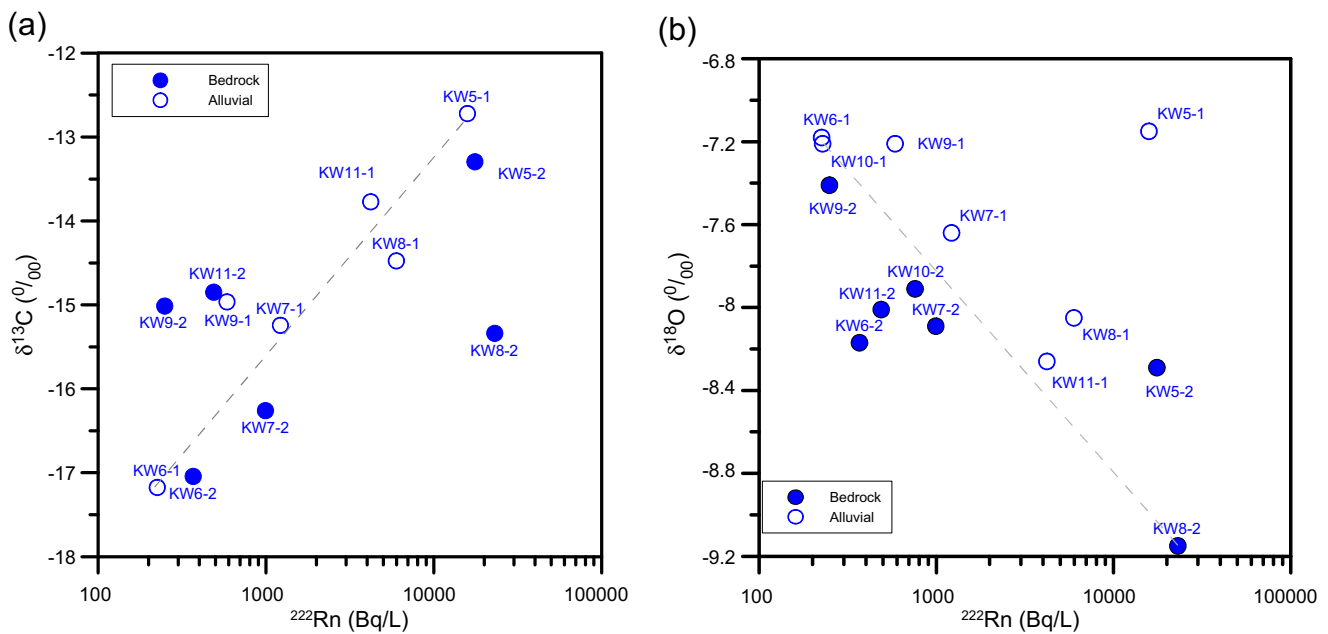


Fig. 9 The concentration of ^{222}Rn versus the values of **a** $\delta^{13}\text{C}$ and **b** $\delta^{18}\text{O}$, in the groundwater samples

observed in KW5-1, KW5-2, KW8-1, and KW11-1 which are located close to the epicenter, indicating that the groundwater was affected by upwelling deep water. The values of $\delta^{18}\text{O}$ and ^{222}Rn are compared in Fig. 9b. The groundwater samples with higher concentrations of ^{222}Rn (KW5-2, KW8-2, KW8-1, and KW11-1) showed depleted values of $\delta^{18}\text{O}$, further indicating that the samples were affected by upwelling deep water.

Discussion

In this study, geochemical and hydrological data were evaluated to understand the responses to an earthquake of aquifers of different types, lithologies, and distances from the epicenter. Groundwater level changes were not observed in most alluvial wells after the earthquake, while groundwater levels and EC increased in the confined igneous rock aquifer for several days to months. The concentrations of Ca^{2+} , Na^+ , SO_4^{2-} , and HCO_3^- increased in groundwater from the bedrock aquifer compared to the alluvial aquifer after the earthquake. Environmental tracer data suggest upwelling of old groundwater and mixing with shallow groundwater in several wells following the earthquake. Depleted values of $\delta^{18}\text{O}$ and δD were observed in the wells showing increased groundwater levels, indicating mixing with upwelling old water. Low concentrations (0.8 TU) of ^3H in the shallow alluvial aquifer also suggest that shallow wells were affected by upwelling deep water with an old water component. Deep and old water was transported to the alluvial aquifer composed of pebbles, up to 8 m below the surface, from the deep aquifer composed of

conglomerate, which can be facilitated by preferential flow paths formed by the earthquake. Higher $^3\text{He}/^4\text{He}$ in KW5-2 and KW7-2 in the bedrock aquifer could possibly be explained by the addition of mantle He sources closely located in the reversal fault in the eastern part of the study area. In contrast, the lower $^3\text{He}/^4\text{He}$ ratios in KW8-2 and KW11-2 could be caused by radiogenic crustal He in the aquifer; these wells are closely located to the slide slip fault in the western part of the study area composed of granite and gneiss.

Cluster analysis was conducted to group wells with similar hydrogeochemical properties using environmental tracer data ($\delta^{18}\text{O}$, δD , $^3\text{He}/^4\text{He}$, $^{20}\text{Ne}/^4\text{He}$, ^3H , ^{222}Rn , and $\delta^{13}\text{C}$). The resulting clustered groups can categorize groundwater in the aquifer system. The clustered groups are presented in the form of a heat map (Fig. 10) and spatial distributions of clustered groups are shown in Fig. 11. Group A is composed of KW5-1, KW5-2, KW7-1, KW7-2, KW8-1, KW8-2, and KW11-1, which all showed high correlations between environmental tracer data, indicating responses to the earthquake (Fig. 10). Group B is composed of KW9-1 and KW11-2, which showed moderate correlations between environmental tracer data, suggesting moderate responses to the earthquake compared to group A (Fig. 10). Group C includes the remaining wells, KW6-1, KW6-2, and KW9-2, which showed a lower correlation between environmental tracer data suggesting less response to the earthquake compared to groups A and B.

Wells in group A were qualitatively assessed to understand the influence of the earthquake on each well. The values of $\delta^{18}\text{O}$ and δD in groundwater samples from the

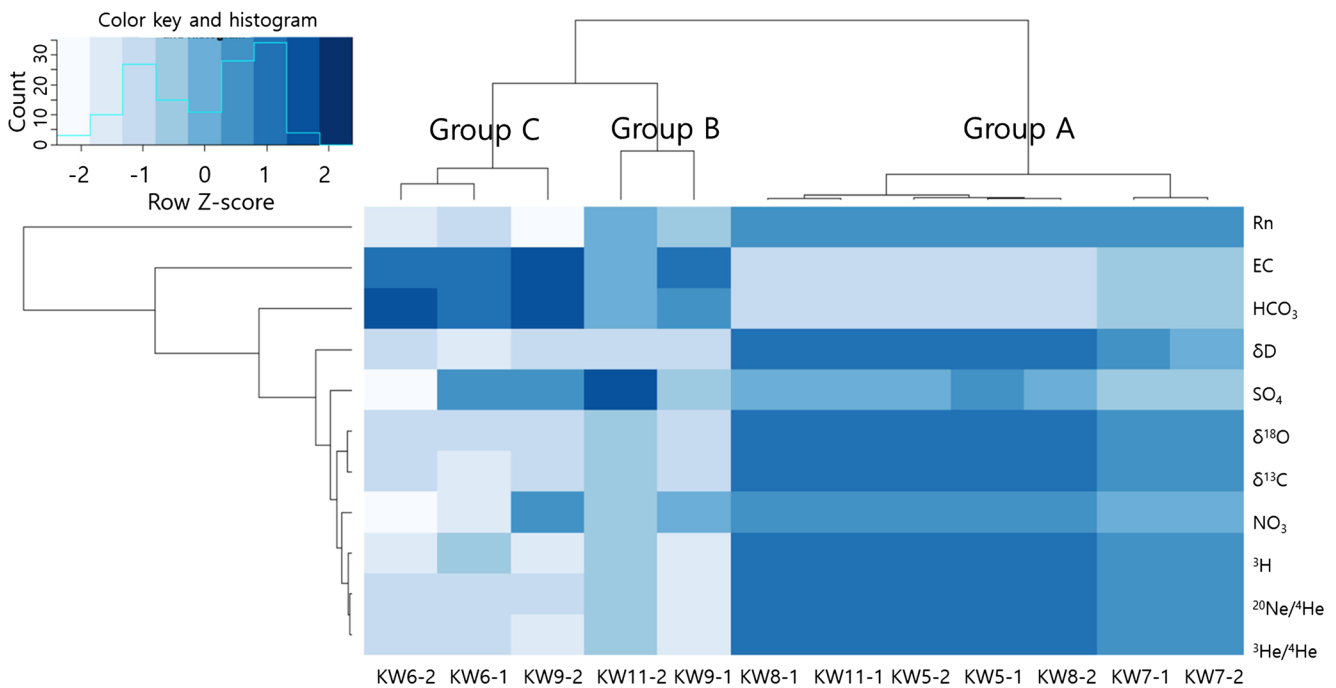


Fig. 10 Dendrogram of the cluster analysis. The low values of the z-score are in shades of light blue to dark blue in the heat map

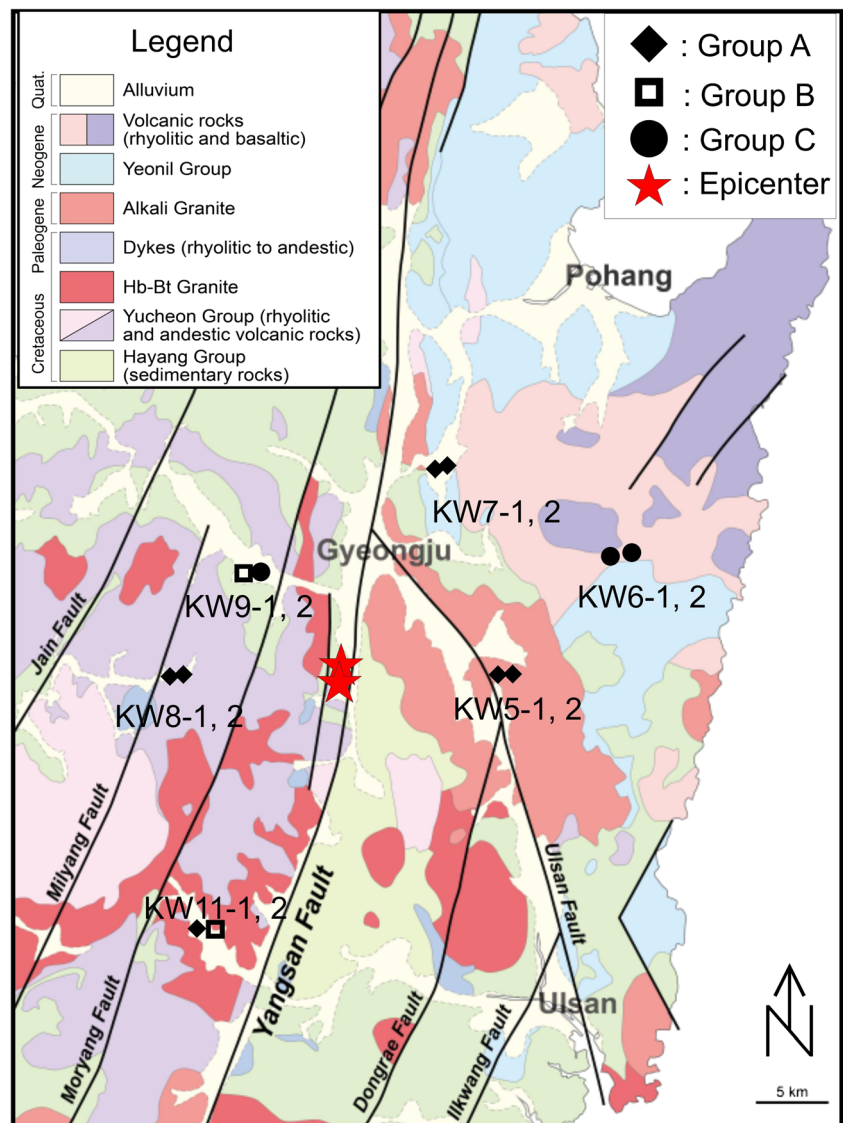
confined bedrock aquifers (KW5-2, KW8-2, and KW11-2) were depleted (Fig. 3). Groundwater samples collected in KW7-1, KW8-1, and KW11-1 installed in the shallow aquifer also showed depleted values of $\delta^{18}\text{O}$ and δD , suggesting mixing with upwelling deep water. High radiogenic helium sources were observed in the confined aquifers composed of igneous rock (KW8-2 and KW11-2) after the earthquake. The concentrations of ^3H showed consistent results with the noble gas data in KW8-2 and KW11-2. A high concentration of ^{222}Rn was observed in the aquifer composed of igneous rock (KW8-2) and mudstone (KW5-2), which is consistent with the $^3\text{He}/^4\text{He}$ data in those wells.

Mantle-originated helium was observed in the aquifer (KW5 and KW7) composed of sedimentary rock (mudstone and conglomerate) which was affected by preferential flow paths, possibly due to the earthquake on the reversal fault (Fig. 5b). Similar $^3\text{He}/^4\text{He}$ ratios, tritium concentrations, and $\delta^{18}\text{O}$ and δD values were observed in the shallow aquifer composed of pebbles (KW7-1) and the deep aquifer composed of conglomerate (KW7-2). The concentration of ^3H in both wells was below 0.8 TU, indicating that groundwater from the deep aquifer intruded to the shallow aquifer possibly due to the earthquake because the location of KW7 is close to the Ulsan Fault, which experienced a high frequency of earthquake aftershocks (Kim et al. 2016) even though the wells are not close to the epicenter. The terrigenic He signatures in groundwater after the earthquakes may be related to the presence of

concealed active faults in the study area, in particular in strata near KW5 and KW7 that contains mantle He (Umeda and Ninomiya 2009; Aydın et al. 2015). This also suggests that further study involving helium isotopes may be helpful to evaluate the characteristics of numerous faults in southeastern Korea; such studies have, so far, been carried out based on mineralogical analysis and field surveys (Jeong and Cheong 2005; Choi et al. 2014).

Groundwater level increased after the earthquake in KW8-2 and environmental tracers including $\delta^{18}\text{O}$, δD , ^3H , ^{222}Rn , and $\delta^{13}\text{C}$ indicated the influence of upwelling water. Environmental tracers in groundwater of KW5-1, KW5-2, and KW7-1 also indicated the influence of upwelling water even though no groundwater level change was observed after the earthquake in those wells (Table 2). It is noteworthy that there was a large groundwater level change in well KW11-2, while environmental tracer concentrations were not significantly affected by upwelling of old water after the earthquake. This result can be explained by the fact that KW11-2 is screened in a confined aquifer in the slide slip fault composed of igneous rock, and thus the geochemistry was less affected by the upwelling of old water compared to the sedimentary rock aquifer closely located in the reversal fault, represented by KW7-2, since earthquakes play an important role in forming preferential flow paths (Kulongoski et al. 2005; Newell et al. 2015; Wei et al. 2015; Batlle-Aguilar et al. 2017). This indicated that hydrological and geochemical data should be carefully evaluated to comprehensively understand the responses of aquifer systems to earthquakes.

Fig. 11 Spatial distribution of clustered groups using environmental tracer data in the study area



Conclusions

In this study, time series data of groundwater levels, electrical conductivity (EC), and geochemical data and environmental tracers, including noble gases, $\delta^{18}\text{O}$, δD , ^3H , ^{222}Rn , and $\delta^{13}\text{C}$, were evaluated to understand the hydrologic and geochemical response to an earthquake in the shallow (alluvial) and deep (bedrock) aquifer. Noble gas anomalies in groundwater after the earthquake were closely related to the fault type, epicentral distance, lithology, and aquifer type. The different distribution of $^3\text{He}/^4\text{He}$ in groundwater from the alluvial and bedrock aquifers indicated crustal mixing in groundwater of the slide slip fault or upwelling of deep water in the reversal fault. Elevated concentrations of ^{222}Rn and enriched values of $\delta^{13}\text{C}$ -DIC were observed in the aquifers located close to the epicenter, also representing the influence of deep water. The resulting groups from the cluster analysis based on environmental tracer data were closely related to the effects of the earthquake on the

aquifer, the characteristics of the faults, and the epicentral distance. Groundwater level and geochemical response after the earthquake showed different correlations depending on the preferential flow path due to aquifer and fault types. Environmental tracer data combined with groundwater level, EC, and geochemical changes can be usefully applied to understand the hydrogeologic and geochemical response to earthquakes in different aquifer types with varying geology. This study also suggests that hydrological and geochemical data should be simultaneously studied to fully understand the response of aquifer systems to earthquakes.

Acknowledgements Suggestions provided by Dr. Rolf Kipfer at the Swiss Federal Institute of Aquatic Science and Technology are kindly acknowledged.

Funding information This study was supported by the National Research Council of Science & Technology (NST) grant by the Korea government (MSIP; No. CAP-17-05-KIGAM).

References

- Amoruso A, Crescentini L, Petitta M, Rusi S, Tallini M (2011) Impact of the 6 April 2009 L'Aquila earthquake on groundwater flow in the Gran Sasso carbonate aquifer, central Italy. *Hydrol Process* 25: 1754–1764
- Andrén M, Stockmann G, Skelton A, Sturkell E, Mörtz C, Guðrúnardóttir HR, Keller NS, Odling N, Dahrén B, Broman C, Balic-Zunic T, Hjartarson H, Siegmund H, Freund F, Kockum I (2016) Coupling between mineral reactions, chemical changes in groundwater, and earthquakes in Iceland. *J Geophys Res Solid Earth* 121:2315–2337. <https://doi.org/10.1002/2015JB012614>
- Aydın H, Hilton DR, Güleç N, Mutlu H (2015) Post-earthquake anomalies in He–CO₂ isotope and relative abundance systematics of thermal waters: the case of the 2011 Van earthquake, eastern Anatolia, Turkey. *Chem Geol* 411:1–11
- Barberio MD, Barbieri M, Billi A, Doglioni C, Petitta M (2017) Hydrogeochemical changes before and during the 2016 Amatrice–Norcia seismic sequence (central Italy). *Sci Rep* 7:11735. <https://doi.org/10.1038/s41598-017-11990-8>
- Batlle-Aguilar J, Banks EW, Batelaan O, Kipfer R, Brennwald MS, Cook PG (2017) Groundwater residence time and aquifer recharge in multilayered, semi-confined and faulted aquifer systems using environmental tracers. *J Hydrol* 546:150–165
- Bauer SJ, Gardner WP, Lee H (2016) Release of radio-genic noble gases as a new signal of rock deformation. *Geophys Res Lett* 43:10,688–10,694. <https://doi.org/10.1002/2016GL070876>
- Chang KH (1975) Cretaceous stratigraphy, sedimentation and tectonics of southeastern Korea (in Korean with English abstract). *J Geol Soc Korea* 13:76–90
- Choi SJ, Jeon JS, Choi JH, Kim B, Ryoo CR, Hong DG, Chwae U (2014) Estimation of possible maximum earthquake magnitudes of Quaternary faults in the southern Korean Peninsula. *Quat Int* 344: 53–63
- Chough SK, Sohn YK (2010) Tectonic and sedimentary evolution of a cretaceous continental arc-back arc system in the Korean peninsula: new view. *Earth Sci Rev* 101:225–249
- Claesson L, Skelton A, Graham C, Dietl C, Morth M, Torssander P, Kockum I (2004) Hydrogeochemical changes bedfore and after a major earthquake. *Geology* 32(8):641–644
- Crossey LJ, Karlstrom KE, Springer AE, Newell D, Hilton DR, Fischer T (2009) Degassing of mantle-derived CO₂ and He from springs in the southern Colorado Plateau region–Neotectonic connections and implications for groundwater systems. *Geol Soc Am Bull* 121(7–8): 1034–1053
- Elkhoury JE, Brodsky EE, Agnew DC (2006) Seismic waves increase permeability. *Nature* 44:1135–1138
- Galassi D, Lombardo P, Fiasca B, Cioccio A, Lorenzo T, Petitta M, Carlo P (2014) Earthquakes trigger the loss of groundwater biodiversity. *Sci Rep* 4:6273. <https://doi.org/10.1038/srep06>
- Gau H, Chen T, Chen J, Liu C (2007) Time series decomposition of groundwater level changes in wells due to the Chi-Chi earthquake in Taiwan: a possible hydrological precursor to earthquakes. *Hydrol Process* 21:510–524
- Hong T, Lee J, Kim W, Hahn I, Woo N, Park S (2017) The 12 September 2016 M_f 5.8 midcrustal earthquake in the Korean peninsula and its seismic implications. *Geophys Res Lett* 44:3131–3138. <https://doi.org/10.1002/2017GL072899.273>
- Igarashi G, Saeki S, Takahata N, Sumikawa K, Tasaka S, Sasaki Y, Takahashi M, Sano Y (1995) Ground-water radon anomaly before the Kobe earthquake in Japan. *Science* 269:60–61
- Ingebritsen SE, Manga M (2014) Earthquakes: hydrogeochemical precursor. *Nat Geosci* 7:697–698
- Jeong GY, Cheong CS (2005) Recurrent events on a Quaternary fault recorded in the mineralogy and micromorphology of a weathering profile, Yangsan fault system, Korea. *Quat Res* 64(2):221–233
- Kaown D, Hyun Y, Bae G, Lee K (2007) Factors affecting the spatial pattern of nitrate contamination in shallow groundwater. *J Environ Qual* 36:1479–1487
- Kaown D, Koh D, Lee K (2009) Effects of groundwater residence time and recharge rate on nitrate contamination deduced from $\delta^{18}\text{O}$, δD , $^3\text{H}/^3\text{He}$ and CFCs in a small agricultural area in Chuncheon Korea. *J Hydrol* 366:101–111
- Kaown D, Koh D, Solomon DK, Yoon Y, Yang J, Lee K (2014) Delineation of recharge patterns and contaminant transport using $3\text{H}-3\text{He}$ in a shallow aquifer contaminated by chlorinated solvents in South Korea. *Hydrogeol J* 22:1041–1054
- Kaown D, Koh E, Mayer B, Kim H, Park D, Park B, Lee K (2018) Application of multiple-isotope and groundwater-age data to identify factors affecting the extent of denitrification in a shallow aquifer near a river in South Korea. *Hydrogeol J* 26:2009–2020
- Kim H, Kaown D, Mayer B, Lee J, Lee K (2018) Combining pyrosequencing and isotopic approaches to assess denitrification in a hyporheic zone. *Sci Total Environ* 631–632:755–764
- Kim NJ, Kwon YI, Jin MS (1971) Geological map of the Morayng sheet (1:50,000). Geological Survey of Korea, Seoul
- Kim Y, Rhie J, Kang K, Kim K, Kim M, Lee S (2016) The 12 September 2016 Gyeongju earthquakes: 1. observation and remaining questions. *Geosci J* 20(6):747–752
- King C, Azuma S, Ohno M, Asai Y, He P, Kitagawa Y, Igarashi G, Wakita H (2000) In search of earthquake precursors in the water-level data of 16 closely clustered wells at Tono, Japan. *Geophys J Int* 143:469–477
- Kipfer R, Aeschbach-Hertig W, Peeters F, Stute M (2002) Noble gases in lakes and ground waters. In: Porcelli D, Ballentine C, Wieler R (eds) Noble gases in geochemistry and cosmochemistry. *Rev Mineral Geochem* 47:615–700
- Koh D, Ha K, Lee K, Yoon Y, Ko K (2012) Flow paths and mixing properties of groundwater using hydrogeochemistry and environmental tracers in the southwestern area of Jeju volcanic island. *J Hydrol* 432–433:61–74
- Koh E, Lee E, Kaown D, Green CT, Koh D, Lee K, Lee S (2018) Comparison of groundwater age models for assessing nitrate loading, transport pathways, and management options in a complex aquifer system. *Hydrol Process* 32:923–938
- Kulongoski JT, Hilton DR, Izbicki JA (2005) Source and movement of helium in the eastern Morongo groundwater basin: the influence of regional tectonics on crustal and mantle helium fluxes. *Geochim Cosmochim Acta* 69(15):3857–3872
- Lee J (2016) Gyeongju earthquakes recorded in daily groundwater data at national groundwater monitoring stations in Gyeongju. *J Soil Groundwater Environ* 21(6):80–86
- Lee K, Jin YG (1991) Segmentation of the Yangsan fault system: geophysical studies on major faults in the Kyeongsang Basin. *J Geol Soc Korea* 27:434–449
- Lee KS, Lee CB (1999) Oxygen and hydrogen isotope composition of precipitation and river waters in South Korea. *J Geol Soc Korea* 35(1):73–84
- Lee S, Ha K, Hamm S, Ko K (2013) Groundwater responses to the 2011 Tohoku earthquake on Jeju Island, Korea. *Hydrol Process* 27:1147–1157
- Lehmann BE, Love A, Purtschert R, Collon P, Loosli HH, Kutschera W, Beyerle U, Aeschbach-Hertig W, Kipfer R, Frapet SK, Herczeg A, Moran J, Tolstikhin IN, Gröning M (2003) A comparison of groundwater dating with ^{81}Kr , ^{36}Cl and ^4He in four wells of the great Artesian Basin, Australia. *Earth Planet Sci Lett* 211:237–250. [https://doi.org/10.1016/S0012-821X\(03\)00206-1](https://doi.org/10.1016/S0012-821X(03)00206-1)

- Liu C, Chia Y, Chuang P, Chiu Y, Tseng T (2018) Impacts of hydrogeological characteristics on groundwater-level changes induced by earthquakes. *Hydrogeol J* 26:451–465
- Manga M (2001) Origin of postseismic streamflow changes inferred from baseflow recession and magnitude-distance relation. *Geophys Res Lett* 28:2133–2136. <https://doi.org/10.1029/2000GL012481>
- Manga M, Wang C (2007) Earthquake hydrology in treatise on geophysics, vol 4, 2nd edn. Elsevier, Amsterdam, pp 293–320
- Montgomery DR, Manga M (2003) Streamflow and water well responses to earthquakes. *Science* 300:2047–2049
- Newell DL, Jessup MJ, Hilton DR, Shaw CA, Hughes CA (2015) Mantle-derived helium in hot springs of the cordillera Blanca, Peru: implications for mantle-to-crust fluid transfer in a flat-slab subduction setting. *Chem Geol* 417:200–209
- Niwa M, Takeuchi R, Onoe H, Tsuyuguchi K, Asamori K, Umeda K, Sugihara K (2012) Groundwater pressure changes in Central Japan induced by the 2011 off the Pacific coast of Tohoku earthquake. *Geochem Geophys Geosyst* 13:Q05020. <https://doi.org/10.1029/2012GC004052>
- Orihara Y, Kamogawa M, Nagao T (2014) Preseismic changes of the level and temperature of confined groundwater related to the 2011 Tohoku earthquake. *Sci Rep* 4:6907. <https://doi.org/10.1038/srep06907>
- Pavin M, Tadakuma N, Asaue H, Koike K (2014) Delineation and interpretation of spatial coseismic response of groundwater levels in shallow and deep parts of an alluvial plain to different earthquakes: a case study of the Kumamoto City area, southwest Japan. *J Asian Earth Sci* 83:35–47
- Petitta M, Mastroiello L, Preziosi E, Banzato F, Barberio M, Billi A, Cambi C, De Luca G, Di Carlo G, Di Curzio D, Di Salvo C, Nanni T, Palpacelli S, Rusi S, Saroli M, Tallini M, Tazioli A, Valigi D, Vivalda P, Doglioni C (2018) Water-table and discharge changes associated with the 2016–2017 seismic sequence in central Italy: hydrogeological data and a conceptual model for fractured carbonate aquifers. *Hydrogeol J* 26:1009–1026
- Reddy DV, Nagabhushanam P (2012) Chemical and isotopic seismic precursory signatures in deep groundwater: cause and effect. *Appl Geochem* 27:2348–2355
- Reddy DV, Nagabhushanam P, Sukhija BS (2011) Earthquake (*M* 5.1) induced hydrogeochemical and $\delta^{18}\text{O}$ changes: validation of aquifer breaching—mixing model in Koyna, India. *Geophys J Int* 184:359–370
- Saby M, Larocque M, Pinti DL, Barbécot F, Sano Y, Castro MC (2016) Linking groundwater quality to residence times and regional geology in the St. Lawrence Lowlands, southern Quebec, Canada. *Appl Geochem* 65:1–13
- Sano Y, Kagoshima T, Takahata N, Nishio Y, Roulleau E, Pinti DL, Fischer TP (2015) Ten-year helium anomaly prior to the 2014 Mt Ontake eruption. *Sci Rep* 5:13069. <https://doi.org/10.1038/srep13069>
- Sano Y, Takahata N, Kagoshima T, Shibata T, Onouem T, Zhao D (2016) Groundwater helium anomaly reflects strain change during the 2016 Kumamoto earthquake in southwest Japan. *Sci Rep* 6:37939. <https://doi.org/10.1038/srep37939>
- Schlosser P, Stute M, Dörr H, Sonntag C, Münnich KO (1988) Tritium/ ^3He dating of shallow groundwater. *Earth Planet Sci Lett* 89 (3–4): 353–362
- Shi Z, Wang G (2015) Sustained groundwater level changes and permeability variation in a fault zone following the 12 May 2008, mw 7.9 Wenchuan earthquake. *Hydrol Process* 29:2659–2667
- Skelton A, Andrén M, Kristmannsdóttir H, Stockmann G, Mörth C, Sveinbjörnsdóttir A, Jónsson S, Sturkell E, Guðrúnardóttir R, Hjartarson H, Siegmund H, Kockum I (2014) Changes in groundwater chemistry before two consecutive earthquakes in Iceland. *Nat Geosci* 7:752–755
- Solomon DK, Cook PG (2000). ^3H and ^3He . In: Cook G, Herzeg AL (eds) Environmental tracers in subsurface hydrology. Springer, Boston. p 397–424
- Song SR, Chen YL, Liu CM, Ku WY, Chen HF, Liu YJ, Kuo LW, Yang TF, Chen CH, Liu TK, Lee M (2005) Hydrochemical changes in spring waters in Taiwan: implications for evaluating sites for earthquake precursory monitoring. *Terr Atmos Ocean Sci* 16:745–762
- Tolstikhin IN, Lehmann BE, Loosli HH, Gautschi A (1996) Helium and argon isotopes in rocks, minerals, and related groundwaters: a case study in northern Switzerland. *Geochim Cosmochim Acta* 60:1497–1514. [https://doi.org/10.1016/0016-7037\(96\)00036-1](https://doi.org/10.1016/0016-7037(96)00036-1)
- Tomonaga Y, Marzocchi R, Pera S, Pfeifer H, Kipfer R, Decrouy L, Vennemann T (2017) Using noble-gas and stable-isotope data to determine groundwater origin and flow regimes: application to the Ceneri Base tunnel (Switzerland). *J Hydrol* 545:395–409
- Torgersen T, Clarke WB (1985) Helium accumulation in groundwater. I: an evaluation of sources and the continental flux of crustal ^4He in the great Artesian Basin, Australia. *Geochim Cosmochim Acta* 49(5):1211–1218. [https://doi.org/10.1016/0016-7037\(85\)90011-0](https://doi.org/10.1016/0016-7037(85)90011-0)
- Umeda K, Ninomiya A (2009) Helium isotopes as a tool for detecting concealed active faults. *Geochem Geophys Geosyst* 10:Q08010. <https://doi.org/10.1029/2009GC002501>
- Wang C, Manga M (2010) Hydrologic responses to earthquakes and a general metric. *Geofluid* 10:201–216
- Wei W, Aeschbach-Hertig W, Chen Z (2015) Identification of He sources and estimation of He ages in groundwater of the North China Plain. *Appl Geochem* 63:182–189. <https://doi.org/10.1016/j.apgeochem.2015.08.010>
- Weise SM, Bräuer K, Kämpf H, Strauch G, Koch U (2001) Transport of mantle volatiles through the crust traced by seismically released fluids: a natural experiment in the earthquake swarm area Vogtland/NW Bohemia, Central Europe. *Tectonophysics* 336(1): 137–150
- Yan R, Woith H, Wang R (2014) Groundwater level changes induced by the 2011 Tohoku earthquake in China mainland. *Geophys J Int* 199(1):533–548. <https://doi.org/10.1093/gji/ggu196>